The cbb_3-type cytochrome oxidase assembly factor CcoG is a widely distributed cupric reductase

Dorian Marckmann[a,1], Petru-Iulian Trasnea[b,1], Johannes Schimpf[c], Christine Winterstein[b], Andreea Andrei[a,d], Stefan Schmollinger[e], Crysten E. Blaby-Haas[f], Thorsten Friedrich[c], Fevzi Daldal[b,2], and Hans-Georg Koch[a,2]

[a]Institute of Biochemistry and Molecular Biology, Zentrum für Biochemie und Molekulare Zellforschung, Faculty of Medicine, Albert Ludwigs University of Freiburg, 79104 Freiburg, Germany; [b]Department of Biology, University of Pennsylvania, Philadelphia, PA 19104; [c]Institute of Biochemistry, Faculty of Chemistry and Pharmacy, Albert Ludwigs University of Freiburg, 79104 Freiburg, Germany; [d]Faculty of Biology, Albert Ludwigs University of Freiburg, 79104 Freiburg, Germany; [e]Department of Plant & Microbial Biology, University of California, Berkeley, CA 94720; and [f]Biology Department, Brookhaven National Laboratory, Upton, NY 11973

Edited by Amy C. Rosenzweig, Northwestern University, Evanston, IL, and approved September 6, 2019 (received for review August 12, 2019)

Copper (Cu)-containing proteins execute essential functions in prokaryotic and eukaryotic cells, but their biogenesis is challenged by high Cu toxicity and the preferential presence of Cu(II) under aerobic conditions, while Cu(I) is the preferred substrate for Cu chaperones and Cu-transport proteins. These proteins form a coordinated network that prevents Cu accumulation, which would lead to toxic effects such as Fenton-like reactions and mismetalation of other metalloproteins. Simultaneously, Cu-transport proteins and Cu chaperones sustain Cu(I) supply for cuproprotein biogenesis and are therefore essential for the biogenesis of Cu-containing proteins. In eukaryotes, Cu(I) is supplied for import and trafficking by cell-surface exposed metalloreductases, but specific cupric reductases have not been identified in bacteria. It was generally assumed that the reducing environment of the bacterial cytoplasm would suffice to provide sufficient Cu(I) for detoxification and cuproprotein synthesis. Here, we identify the proposed cbb_3-type cytochrome *c* oxidase (cbb_3-Cox) assembly factor CcoG as a cupric reductase that binds Cu via conserved cysteine motifs and contains 2 low-potential [4Fe-4S] clusters required for Cu(II) reduction. Deletion of *ccoG* or mutation of the cysteine residues results in defective cbb_3-Cox assembly and Cu sensitivity. Furthermore, anaerobically purified CcoG catalyzes Cu(II) but not Fe(III) reduction in vitro using an artificial electron donor. Thus, CcoG is a bacterial cupric reductase and a founding member of a widespread class of enzymes that generate Cu(I) in the bacterial cytosol by using [4Fe-4S] clusters.

cytochrome oxidase | copper | membrane protein biogenesis | *Rhodobacter capsulatus* | homeostasis

Copper (Cu) is an essential micronutrient for all domains of life. Its physicochemical properties render this transition metal a redox cofactor commonly found in many enzymes catalyzing oxygen-linked reactions, including the dopamine β-hydroxylases, Cu-Zn superoxide dismutases, multicopper oxidases, and the superfamily of heme-copper oxygen reductases (1, 2). The redox properties of Cu are also responsible for its cytotoxicity. In the presence of reactive oxygen species, it can generate hydroxyl radicals that damage DNA, lipids, and proteins (3). Moreover, because of its high thiophilicity (4), it can replace other transition metals (e.g., iron) in proteins, leading to their inactivation (5). In humans, imbalanced copper homeostasis is associated with severe diseases, including Wilson's disease, Menkes disease, Alzheimer's disease, prion disease, and atherosclerosis (6). Cells reduce the risk of Cu toxicity by using sophisticated acquisition, chaperoning, and storage systems to tightly control its amount while allowing its availability for cuproprotein biosynthesis (1, 2).

P_{1B}-type ATPases, like ATP7A and ATP7B in eukaryotes and CcoI and CopA in bacteria, are central for Cu homeostasis and transport Cu(I) for detoxification and cuproprotein biosynthesis. Under aerobic conditions, Cu(II) is the predominant Cu species, which links Cu transport inevitably to Cu(II) reduction. Multiple Cu-reducing enzymes are known in eukaryotes. They primarily reduce Fe(III) to Fe(II) (7), but proteins like Fre1p/Fre2p (8), Dcytb (9), or STEAP (6-transmembrane epithelial antigen of the prostate) family members (10) also reduce Cu(II) to Cu(I). These metalloreductases contain heme and flavins, and use reductants like NAD(P)H for Cu(II) or Fe(III) reduction. They are localized in the plasma membrane with the reductase domain facing the extracellular side, linking them to Fe(II) import via IRT or NRAMP, or Cu(I) import via Ctr1 (7). In the cytoplasm, Cu(I) is bound by Cu chaperones like yeast or human Atox1 (Hah1) which maintain Cu(I) in the reduced state and deliver it to P_{1B}-type ATPases at the endoplasmic reticulum for cuproprotein synthesis (11).

There are few studies on Cu(II) reduction in prokaryotes, and they mainly describe nonenzymatic reactions via membrane-bound quinones. Examples are a cupric reductase activity in intact *Lactobacillus lactis* cells (12) or the cupric reductase activity of *Escherichia coli* NADH dehydrogenase 2 (13, 14). Importantly, no specific cytoplasm-exposed cupric reductase has been identified in eukaryotes or bacteria so far (7, 15). It is generally assumed that Cu(II) entering the cytoplasm would be converted spontaneously to Cu(I) in this reducing environment. Hence, no specific cytoplasmic cupric reductase would be required.

Significance

Copper (Cu) is a cofactor of many enzymes in prokaryotes and eukaryotes, but Cu toxicity challenges cuproprotein biogenesis. To prevent Cu-induced damage while sustaining Cu supply for cuproproteins, cells possess sophisticated Cu transport and storage networks. P_{1B}-type ATPases and Cu chaperones are central to these networks and preferentially bind Cu(I). However, under aerobic conditions, Cu exists primarily as Cu(II), and hence Cu(II) reduction is essential for Cu transport/storage. Eukaryotic organisms achieve this process via cell-surface exposed metalloreductases. For bacteria, it was generally assumed that the reducing environment of the cytoplasm would suffice to generate Cu(I). However, our findings now show that this dogma is incomplete, as we have identified a bacterial cupric reductase that reduces Cu(II) in the bacterial cytosol.

Author contributions: D.M., P.-I.T., C.E.B.-H., T.F., F.D., and H.-G.K. designed research; D.M., P.-I.T., J.S., C.W., A.A., S.S., C.E.B.-H., and T.F. performed research; C.W. contributed new reagents/analytic tools; D.M., P.-I.T., J.S., A.A., S.S., C.E.B.-H., T.F., F.D., and H.-G.K. analyzed data; and D.M., P.-I.T., C.E.B.-H., T.F., F.D., and H.-G.K. wrote the paper.

The authors declare no competing interest.

This article is a PNAS Direct Submission.

[1]D.M. and P.-I.T. contributed equally to this work.

[2]To whom correspondence may be addressed. Email: fdaldal@sas.upenn.edu or hans-georg.koch@biochemie.uni-freiburg.de.

This article contains supporting information online at www.pnas.org/lookup/suppl/doi:10.1073/pnas.1913803116/-/DCSupplemental.

First published September 30, 2019.

Intriguingly, the *Archeoglobus fulgidus* copper chaperone CopZ, which delivers Cu(I) to the Cu-exporting P_{1B}-type ATPase CopA, is fused to a low-potential [2Fe-2S]–containing domain that has been implicated in Cu(II) reduction (16). This raises the possibility that cytosolic cupric reductases might exist at least in prokaryotes, but they have been overlooked so far.

In gram-negative bacteria, Cu homeostasis is best characterized in *Rhodobacter capsulatus*, which requires Cu import for the assembly of cbb_3-type cytochrome *c* oxidase (cbb_3-Cox). This enzyme is confined to bacteria and often the sole terminal Cox in several pathogenic species (17, 18). The cbb_3-Cox consists of 3 main subunits, the heme-copper–containing catalytic subunit CcoN, where oxygen is converted to water, and 2 membrane-bound *c*-type cytochromes, CcoO and CcoP, that convey electrons to this catalytic center. In *R. capsulatus* and some other species, 2 additional subunits, CcoQ and CcoH, are also found (19, 20). In *R. capsulatus*, Cu uptake relies on CcoA, which is the first example of a Cu-importing major facilitator superfamily (MFS) protein (21, 22). Intracellular Cu(I) is bound to the cytoplasmic chaperone CopZ (23) and conveyed to the P_{1B}-type ATPase CcoI, transporting Cu(I) back to the periplasm (24). Cu insertion into cbb_3-Cox is then mediated by sequential interactions of 2 periplasmic Cu chaperones, SenC and PccA (homologs of ScoI and PCu_AC, respectively) (25, 26). Excess Cu is transported from the cytoplasm to the periplasm via a second P_{1B}-type ATPase, CopA (27, 28), that exports Cu(I) and thus requires (like CcoI) Cu(II) reduction.

In many bacterial genomes, including *R. capsulatus*, the structural genes (*ccoNOQP*) of cbb_3-Cox are located next to their biogenesis genes (*ccoGHIS*), encoding the subunit CcoH, the Cu transporter CcoI, and the CcoS protein, probably involved in heme insertion into CcoN (29, 30). The first gene of this cluster, *ccoG*, encodes a membrane-integral protein of unknown function (Fig. 1). Earlier, a redox-based role in symbiotic nitrogen fixation for the *Rhizobium meliloti* CcoG homolog FixG (31) and a regulatory role in photosynthetic gene expression for the *Rhodobacter sphaeroides* CcoG homologs RdxA and RdxB (32, 33) have been proposed. Here, we show that CcoG is required for cbb_3-Cox assembly and Cu resistance and contains 2 [4Fe-4S] clusters. Moreover, purified CcoG binds 2 Cu atoms via conserved Cys motifs and exhibits cupric, but not ferric, reductase activity in vitro. Our data reveal that CcoG is a hitherto unknown type of bacterial cupric reductase that catalyzes cytosolic Cu(II) reduction. The widespread occurrence of CcoG homologs among bacterial species implies that spontaneous Cu(II) reduction in the cytosol is inefficient for cbb_3-Cox biogenesis, and cells rely on an enzymatic process that allows sufficient Cu(I) supply for cuproprotein biogenesis and copper homeostasis.

Results

Widespread Occurrence of CcoG-Like Proteins. As with cbb_3-Cox (18, 34), CcoG-like proteins (defined as matching InterPro domain IPR014116) are found predominately in Proteobacteria and Bacteroidetes (Fig. 2). They are typically encoded in genomes that contain a CcoN homolog (defined as matching InterPro domain IPR004677), and most (~80%) of them are located near the genes encoding the subunits and assembly factors of cbb_3-Cox. Curiously, about one-half of the *ccoG*-like genes that are not located near the cbb_3-Cox genes are paralogs and occur in genomes with a second *ccoG*-like gene in a cbb_3-Cox neighborhood. In addition to Proteobacteria and Bacteroidetes, the CcoG-like proteins are also found in most of the Ignavibacteriae and Verrucomicrobia and in some Acidobacteria, Chlorobi, Planctomycetes, and Spirochaetes genomes (Fig. 2). Out of 6,104 bacterial genomes analyzed, 25 contain a CcoG-like protein without any detectable CcoN-like protein (Dataset S1). The occurrence of *ccoG* paralogs that do not belong to cbb_3-Cox neighborhoods and the presence of *ccoG*-like genes in genomes without *ccoN* suggest that CcoG-like proteins might also play an additional role(s) beyond cbb_3-Cox biogenesis.

CcoG Is Required for Optimal Semiaerobic Growth and Copper Homeostasis. The *R. capsulatus* Δ*ccoG* mutant (CW5) shows an NADI-slow (i.e., formation of indophenol blue upon staining of colonies with α-naphthol and dimethyl-4-phenylenediamine [DMPD]) phenotype, suggesting that it contains low cbb_3-Cox activity (29). This phenotype is best observed during the early phase of respiratory growth. Compared with the wild-type strain (MT1131), the Δ*ccoG* mutant exhibits slower growth unless complemented with a wild-type *ccoG* allele (pRKccoG; *SI Appendix*, Fig. S1 *A* and *B* and Table S1). Moreover, the Δ*ccoG* mutant is more sensitive to Cu(II) compared with wild type, as its

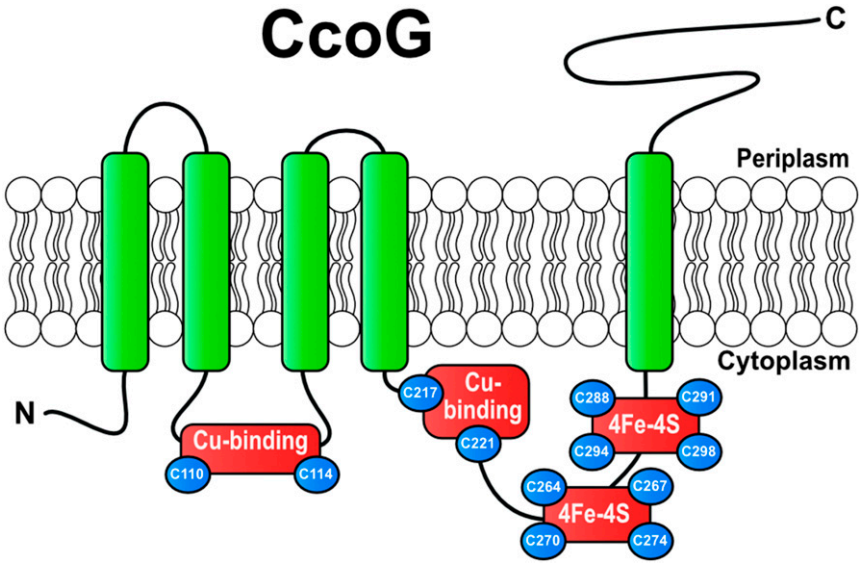

Fig. 1. CcoG protein and its characteristic features. The *R. capsulatus* CcoG protein is depicted with its 5 transmembrane helices, 2 conserved Cu-binding motifs (Cys_{110}-XXX-Cys_{114}) and (Cys_{217}-XXX-Cys_{221}), and 2 conserved [4Fe-4S] cluster-binding motifs (Cys_{264}-XX-Cys_{267}-XX-Cys_{270}-XXX-Cys_{274}) and (Cys_{288}-XX-Cys_{291}-XX-Cys_{294}-XXX-Cys_{298}). Its periplasmic C-terminal portion forms an Ig-like domain.

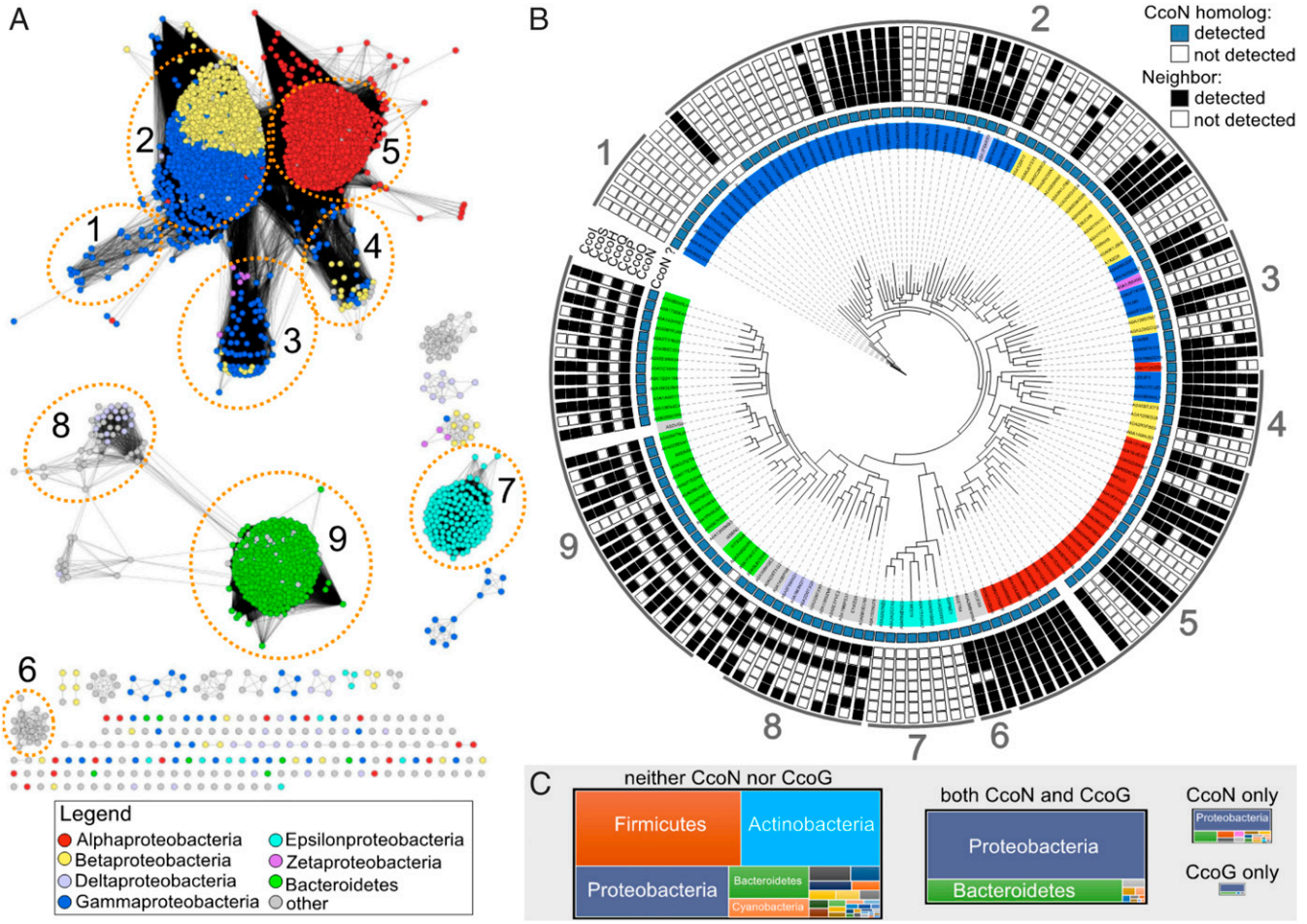

Fig. 2. Phylogenomic analysis of CcoG-like proteins in bacteria. (*A*) Sequence similarity network of proteins in the UniProt database that contain both the 4Fe-4S ferredoxin-type Fe-S–binding domains Fer4_5 (PF12801) and Fer4_18 (PF13746) with and without the Ig-like FixG_C (PF11614) domain, and other proteins that contain the FixG_C domain (domain combinations are indicated in *SI Appendix*, Fig. S8 and Dataset S1). The nodes are colored based on proteobacterial class or if the corresponding organism is from Bacteroidetes. Protein clusters are numbered and correspond to the indicated clades in the tree in *B*. (*B*) Phylogenetic reconstruction of selected (*Materials and Methods*) CcoG-like proteins. Whether a CcoN homolog was detected in the corresponding proteome is indicated with a blue square. The presence of the corresponding *ccoG-like* gene in a neighborhood with genes encoding CcoN, CcoO, CcoP, CcoH, CcoI, CcoS, or CcoQ is indicated with a black box. Correspondence with the network in *A* is indicated by the numbers around the outside of the tree. (*C*) Treemaps illustrating the number of proteomes from each phylum with the indicated presence/absence of CcoN-like and CcoG-like proteins. The size of each treemap is scaled to the overall sum of proteomes for each category.

respiratory growth in enriched medium is inhibited by the presence of ≥200 μM $CuSO_4$ (*SI Appendix*, Fig. S1*C*). Conversely, wild-type cells carrying additional *ccoG* copies show increased Cu resistance (*SI Appendix*, Fig. S1*D*). Thus, the absence of CcoG affects both respiratory growth and Cu tolerance.

***cbb*$_3$-Cox Activity Is Reduced in the Absence of CcoG.** Determination of the whole-cell *cbb*$_3$-Cox activity indicated that the *ΔccoG* mutant has ∼10 to 20% of the wild-type activity during the exponential phase of respiratory growth (Fig. 3*A*). Indeed, its complementation with a wild-type *ccoG* or its FLAG-tagged variant (pRKccoG or pRKccoG$_{Flag}$; *SI Appendix*, Table S2) restored this defect, demonstrating that CcoG is required for full *cbb*$_3$-Cox activity. No major difference in the amounts of the *c*-type cytochrome subunits CcoP and CcoO of *cbb*$_3$-Cox was seen between the membranes from wild-type, *ΔccoG*, or complemented *ΔccoG*-pRKccoG strains (Fig. 3*B*). In contrast, the amounts of the Cu-containing catalytic subunit CcoN were decreased in the absence of CcoG (Fig. 3*C*). Thus, the absence of CcoG affects predominantly the amounts of the Cu-containing CcoN subunit of *cbb*$_3$-Cox.

Four Cysteine Motifs in CcoG Are Essential for Its Function. The CcoG-like proteins have conserved architectures composed of a cytosolic N terminus, 5 transmembrane (TM) helices, and a periplasmic C terminus with a predicted Ig-like domain. They contain 12 invariant cysteine residues clustered into 4 conserved motifs (Fig. 1). The first of these motifs (Cys_{110}-XXX-Cys_{114}-Pro) is in the cytosolic loop between TM2 and TM3, while its duplicate (Cys_{217}-XXX-Cys_{221}-Pro) motif is close to the end of TM4 in the cytosolic loop connecting TM4 and TM5. Similar motifs bind Cu in Sco-like Cu chaperones [e.g., the periplasmic SenC of *R. capsulatus* (35)], further suggesting a role for CcoG in Cu metabolism. In addition, 2 identical motifs (Cys_{264}-XX-Cys_{267}-XX-Cys_{270}-XXX-Cys_{274}) and (Cys_{288}-XX-Cys_{291}-XX-Cys_{294}-XXX-Cys_{298}) are located in the cytoplasmic loop between TM4 and TM5 (Fig. 1). The latter motifs have previously been identified as typical Fe-S cluster-binding sequences (31) and characterized in many ferredoxins. Moreover, the experimentally verified topology of *R. sphaeroides* RdxA (32), a CcoG-like protein, indicates that these metal-binding regions are cytoplasm-exposed. For investigating the functions of the Cys motifs, single Cys-to-Ala substitutions were constructed (on pRKccoG$_{Flag}$;

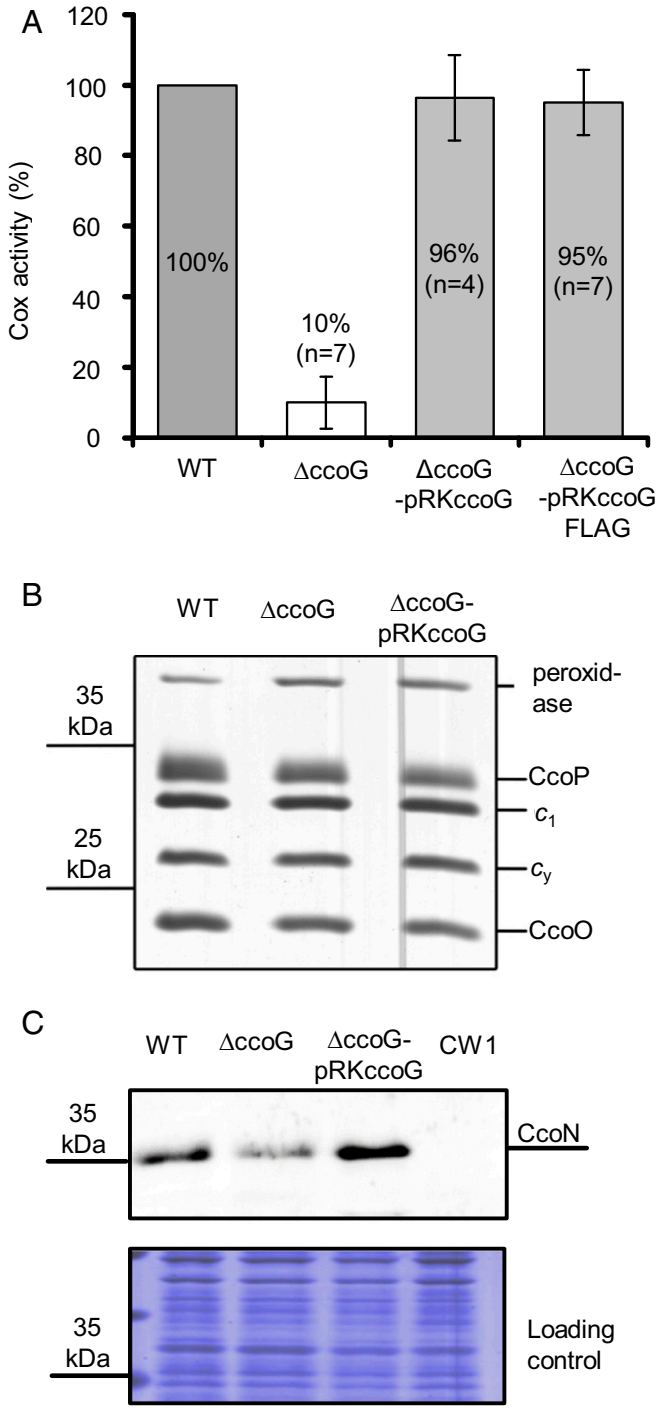

Fig. 3. CcoG is required for cbb_3-Cox activity but not for its assembly. (*A*) The wild-type (WT), knockout (Δ*ccoG*), and complemented (Δ*ccoG-pRKccoG* or Δ*ccoG-pRKccoG*$_{Flag}$) strains (*SI Appendix*, Table S2) were grown under semiaerobic conditions in MPYE medium. The cbb_3-Cox activity was determined by monitoring the DMPD oxidation using intact cells (*Materials and Methods*). The wild-type activity was set to 100% and at least 4 repeat measurements ($n = 4$) were averaged. Statistical analysis was performed on the raw data using the Student's *t* test with $P < 0.0005$ as the level of significance between wild-type and Δ*ccoG* strains. The level of significance between wild-type and the complemented Δ*ccoG* strains was $P > 0.05$ and considered to be not significant. Data are presented as means ± SD. (*B*) The presence of the *c*-type cytochrome subunits CcoP and CcoO of cbb_3-Cox was determined by staining with TMBZ; 50 μg of ICMs was separated using Tricine-SDS/PAGE (*Materials and Methods*). This also visualized all membrane-bound *c*-type cytochromes, including the cytochrome c_1 of the cytochrome bc_1 complex and the membrane-bound electron carrier cytochrome c_y. The experiment was repeated at least 4 times ($n = 4$) and a representative gel with the WT, knockout (Δ*ccoG*), and complemented (Δ*ccoG-pRKccoG*) strains is shown. No difference was seen for the cytochrome c_1 of the cytochrome bc_1 complex, the membrane-bound electron donor cytochrome c_y, or the cytochrome *c* peroxidase, which served as controls. (*C*) The presence of the Cu-containing subunit CcoN of cbb_3-Cox was determined using immunoblotting; 50 μg of ICMs was separated via Tris-SDS/PAGE, membrane-blotted proteins were probed using antibodies against *R. capsulatus* CcoN, and the signal was detected by immunofluorescent secondary antibodies (*Upper*). The experiment was repeated at least 3 times ($n = 3$) and a representative blot (*Upper*) with its loading control (Coomassie-stained gel; *Lower*) is shown. The Δ*ccoGHIS* strain (CW1; *SI Appendix*, Table S2) lacking CcoN was used as a control.

SI Appendix, Table S2), yielding CcoG-Cys$_{110}$Ala in the first, CcoG-Cys$_{221}$Ala in the second, CcoG-Cys$_{267}$Ala in the third, and CcoG-Cys$_{291}$Ala mutants in the fourth motif (Fig. 4*A*, arrows). These mutants are unable to rescue the slow-growth defect of the Δ*ccoG* mutant (Fig. 4*B*). Furthermore, although the mutant proteins were produced in *R. capsulatus* Δ*ccoG* cells, they were unable to restore cbb_3-Cox activity in Δ*ccoG* cells (Fig. 4 *C* and *D*). However, we noted that less of the CcoG-Cys$_{267}$Ala mutants was produced in comparison with the other mutants. Nevertheless, these data indicate that all 4 Cys motifs are required for the function of CcoG in cbb_3-Cox biogenesis.

CcoG Contains Tetranuclear Fe-S Clusters. The presence of a ferredoxin-like low-potential Fe-S cluster(s) in CcoG was further evidenced by X-band, continuous-wave electron paramagnetic resonance (CW-EPR) spectroscopy. Membrane fractions were prepared under anaerobic conditions from CcoG-expressing *E. coli* strains, and strains carrying the empty plasmid served as a control. The EPR spectra recorded at 45 K and 5-mW microwave power of the membranes from both strains were virtually identical, suggesting that CcoG did not contain binuclear Fe-S clusters. However, clear differences were seen in the EPR spectra obtained at 13 K and 10 mW. A difference spectrum was obtained by subtracting the 13 K spectra of the strain lacking CcoG from that producing it (Fig. 5*A*) and interpreted as indicative of the presence of 2 [4Fe-4S] clusters. Based on the saturation behaviors of the individual signals observed by increasing the microwave power, the signals were attributed to one cluster with rhombic symmetry with $g_{x,\ y,\ z} = 1.89$, 1.94, and 2.05, and another cluster with axial symmetry with $g_{//,\ \perp} =$ 2.05 and 1.94 (36). Thus, the EPR data support the proposal that CcoG has 2 tetranuclear Fe-S clusters associated with its specific Cys motifs.

Membranes Containing CcoG Exhibit Cupric Reductase Activity. Since CcoG contains both Cu-binding motifs and ferredoxin-like tetranuclear Fe-S clusters, we inquired whether it can catalyze Cu(II) reduction. Although the cytoplasm is a reducing environment, rapid and specific reduction of Cu(II) to Cu(I) may be crucial especially at the onset of the oxidative growth. We developed an enzymatic assay to monitor Cu(II) reduction by CcoG using *R. capsulatus* membrane fractions prepared under anaerobic conditions (*Materials and Methods*). Air-sensitive kinetics of cupric reductase activity associated with CcoG was monitored spectroscopically via the formation of the Cu(I)–bathocuproine sulfonate (BCS) [Cu(I)–BCS$_2$] complex at 482 nm (Fig. 5*B*). Kinetic traces indicated that membranes of the wild-type strain (MT1131) converted Cu(II) to Cu(I) with a much higher rate [~300 nmol Cu(I)·min^{-1}·mg^{-1} of membrane proteins] than membranes of the Δ*ccoG* mutant [~20 nmol Cu(I)·min^{-1}·mg^{-1} of membrane proteins] (Fig. 5*B*). Upon exposure of the membranes to air, which damages Fe-S clusters (37), the wild-type activity was reduced to that seen in the Δ*ccoG* strain, which remained unaffected (Fig. 5*B*). The origin of the CcoG-independent and

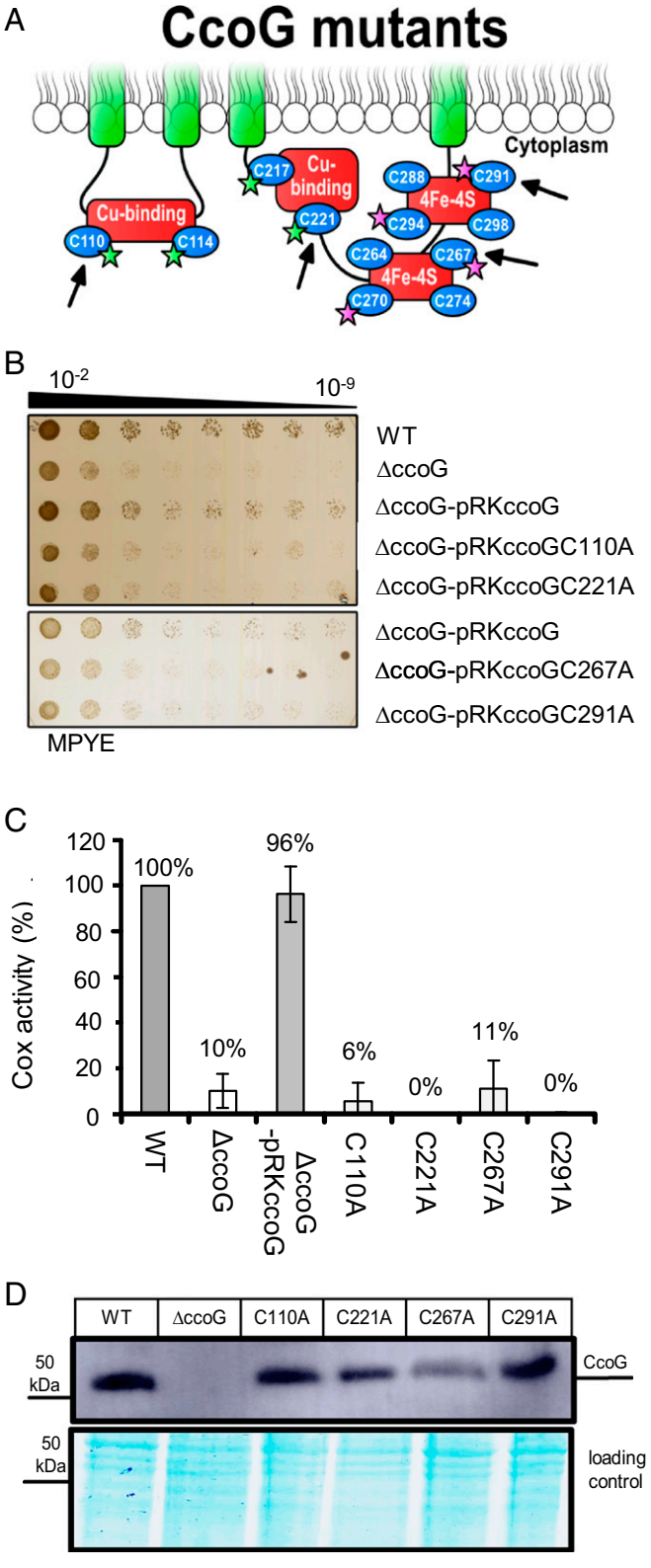

Fig. 4. All 4 cysteine motifs are required for CcoG function. (*A*) A cartoon of CcoG showing its Cu and [4Fe-4S] cluster-binding motifs as red boxes. The single mutants were derivatives of pRKccoG$_{FLAG}$ in *R. capsulatus* (*SI Appendix*, Table S2) and the Cys-to-Ala mutations (C_{110}A, C_{221}A, C_{267}A, and C_{291}A) are indicated by arrows. The quadruple mutants were derivatives of pBADccoG in *E. coli* (*SI Appendix*, Table S2); the CcoG C_{110}, C_{114}, C_{217}, and Cys_{221} residues replaced with Ser are indicated by green stars in the case of CcoG(ΔCu), and the C_{267}, C_{270}, C_{291}, and C_{294} residues replaced with Ser indicated by purple stars in the case of CcoG(ΔFeS) are shown. (*B*) The strains described in *A* were tested for growth on enriched MPYE plates after incubation at 35 °C for about 20 h. A representative set is shown ($n = 3$). (*C*) The cbb_3-Cox activity of the indicated strains was determined as in Fig. 3A. Each activity was measured at least twice in at least 3 independent experiments ($n = 3$). The cbb_3-Cox activity exhibited by the wild-type strain was set to 100%. Statistical analysis was performed on the raw data using the Student's *t* test with $P < 0.0003$ as the level of significance between the wild type and all strains, with the exception of the Δ*ccoG*-pRKccoGC267A ($P < 0.0007$) and Δ*ccoG*-pRKccoG ($P > 0.05$). Data are presented as means ± SD. (*D*) Immunoblot showing that the Cys-to-Ala substitution mutant derivatives of CcoG are produced in *R. capsulatus* (50 μg of membranes was loaded).

air-resistant activity was not investigated further, but could be due to the nonenzymatic Cu reduction that has been observed previously (12, 13). Additional assays using *R. capsulatus* membranes showed that CcoG-dependent cupric reductase activity was proportional to the concentration of Cu(II) and the amount of membranes used (*SI Appendix*, Fig. S2 *A* and *B*). Cupric reductase activity in *R. capsulatus* membranes also required intact Cu- and Fe-S–binding motifs of CcoG (*SI Appendix*, Fig. S2*C*). In addition, similar kinetic data were also obtained by using anaerobically prepared *E. coli* membranes that produced wild-type or CcoG(ΔCu) or CcoG(ΔFeS) mutant proteins (*SI Appendix*, Fig. S2*D*).

Purified CcoG Binds 2 Cu Atoms per Molecule. Next, CcoG and its 2 mutant variants CcoG(ΔCu) and CcoG(ΔFeS) were produced in *E. coli* and purified to homogeneity by affinity chromatography (*Materials and Methods*). In the CcoG(ΔCu) mutant, the Cys_{110}, Cys_{114}, Cys_{217}, and Cys_{221} residues of the (Cys-XXX-Cys-Pro) motifs were replaced with serine (Fig. 4*A*, green stars). Similarly, in the CcoG(ΔFeS) mutant, the Cys_{267}, Cys_{270}, Cys_{291}, and Cys_{294} residues of the predicted [4Fe-4S] cluster-binding motifs were replaced with serine (Fig. 4*A*, purple stars) (*SI Appendix*, Table S1). As expected, the purified CcoG runs as a single band of 55 kDa in sodium dodecyl sulfate–polyacrylamide gel electrophoresis (SDS/PAGE) and exhibits a brownish color (absorption peak at 410 nm) when purified under anaerobic conditions (*SI Appendix*, Fig. S3 *A* and *B*). The metal content of purified CcoG was determined spectrophotometrically and by inductively coupled plasma mass spectrometry (ICP-MS). This revealed the presence of Fe, S, and Cu. However, purified CcoG is slightly substoichiometric in respect to its metal cofactors (*SI Appendix*, Fig. S3*C*), probably due to some oxidative damage of the metal centers during purification.

Next, we measured the Cu-binding stoichiometry of CcoG by using the charge-transfer band at 620 nm of the Cu(II)–thiolate complex formed between CcoG and Cu(II) (Fig. 6*A*). When CcoG was incubated with increasing Cu(II) concentrations, saturation was attained at a CcoG:Cu(II) ratio of 1:2 (Fig. 6*B*), in agreement with its 2 (Cys-XXX-Cys-Pro) motifs (Fig. 1). We also observed a similar CcoG:Cu(II) ratio (1:2) for the CcoG(ΔFeS) variant (*SI Appendix*, Fig. S4 *A* and *B*), but could not detect any charge-transfer band when the CcoG(ΔCu) variant was used (*SI Appendix*, Fig. S4*C*). The data further showed that the 2 cytoplasm-exposed (Cys-XXX-Cys-Pro) motifs of CcoG are required for binding 2 Cu(II) atoms per protein molecule.

CcoG Is a Cupric Reductase. The cupric reductase assay used to monitor Cu(II) reduction with cell membranes (Fig. 5*B*) was extended to purified CcoG and its mutant variants (*Materials and Methods*). Single-turnover assays with dithionite-reduced CcoG from which excess dithionate was removed (*Materials and Methods*) showed that the wild-type protein converted Cu(II) to Cu(I), whereas the CcoG(ΔCu) and CcoG(ΔFeS) mutant variants failed to do so. This activity was sensitive to air or high temperature (90 °C) and proportional to the amount of prereduced protein

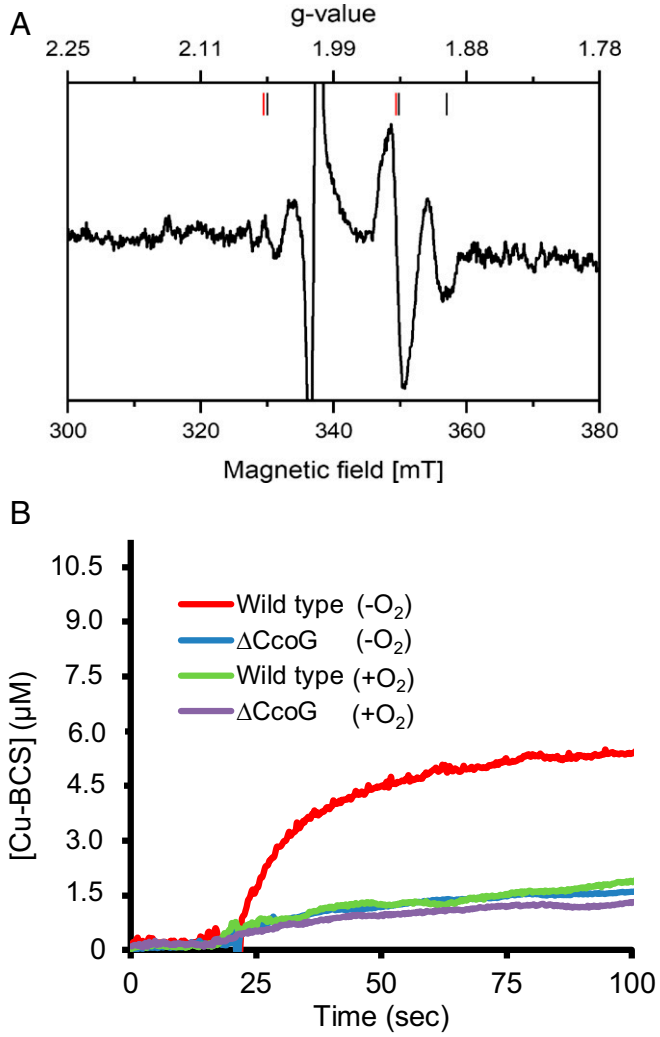

Fig. 5. Membranes containing CcoG have Fe-S clusters and exhibit cupric reductase activity. (*A*) *E. coli* membranes isolated under anaerobic conditions from a strain overproducing CcoG and from one carrying the empty expression plasmid were reduced by addition of a few grains of dithionite, incubated for 30 s, and transferred into an EPR tube. EPR spectra were recorded at 13 K, 10-mW microwave power and with 10 scans. The spectrum obtained with membranes from the strain containing the empty expression plasmid was subtracted from that of the strain overproducing CcoG. The signals attributed to each cluster are indicated by red (axial) and black (rhombic) bars. The large radical signal at $g = 2.0$ due to dithionite reduction is omitted. Other EPR parameters used were: microwave frequency, 9.471 GHz; modulation amplitude, 0.6 mT; time constant, 0.164 s; scan rate, 17.9 mT/min. (*B*) Cupric reductase activity associated with CcoG was measured using anaerobically prepared *R. capsulatus* membranes from wild-type (MT1131) and Δ*ccoG* (CW5) strains (*SI Appendix*, Table S2). In each case, 100 μg of membranes was mixed with 200 μM BCS anaerobically in a sealed cuvette, the assay was initiated by adding 20 μM Cu(II), and the production of the Cu(I)–BCS_2 (Cu–BCS) complex was monitored at 482 nm. The kinetic difference seen between the wild-type and Δ*ccoG* strains reflects the CcoG-dependent cupric reductase activity. As a control, the same assays were repeated after exposing the membranes to air ($+O_2$) to inactivate the O_2-sensitive CcoG-dependent cupric reductase activity. All experiments were repeated at least 3 times ($n = 3$) and a representative trace is shown.

used (*SI Appendix*, Fig. S5 *A–C*). Using the same assay where BCS was substituted with bathophenanthroline sulfonate (BPS), which is a specific Fe^{2+} chelator (*Materials and Methods*), no reduction of Fe^{3+} to Fe^{2+} by prereduced CcoG could be detected (*SI Appendix*, Fig. S5*D*). Thus, purified CcoG protein acts as a specific cupric reductase provided that it is chemically prereduced.

Searches for a suitable electron donor showed that Tris(2-carboxyethyl)phosphine (TCEP), NADPH, and NADH showed no appreciable nonenzymatic Cu(II) reduction in the presence of lecithin (*SI Appendix*, Fig. S6*A*). NADH also did not show significant Cu(II) reduction in the presence of CcoG, while NADPH supported slow CcoG-dependent Cu(II) reduction (*SI Appendix*, Fig. S6*B*). In contrast, when TCEP (10 μM) and lecithin (100 μg/mL) were added to the assay buffer, purified CcoG reduced efficiently Cu(II) to Cu(I) without any need for prereduction [at a rate of ∼2,000 nmol Cu(I)·min^{-1}·mg^{-1} of CcoG, and a k_{cat} of ∼25/min with TCEP as the electron donor], whereas the purified CcoG(ΔCu) and CcoG(ΔFeS) mutant variants could not do so [at rates of ∼30 nmol Cu(I)·min^{-1}·mg^{-1} mutant CcoG] (Fig. 6*C* and *SI Appendix*, Fig. S6*B*). It should be noted that due to the substoichiometric presence of Cu/Fe, the k_{cat} is probably underestimated. Furthermore, no appreciable reduction of Fe^{3+} to Fe^{2+} by purified CcoG was observed via this steady-state assay (Fig. 6*D*). As expected, this activity was sensitive to high temperature (95 °C) and proportional to the amount of protein or Cu(II) concentration used (*SI Appendix*, Fig. S7). The overall data established that purified CcoG has cupric, but not ferric, reductase activity in the presence of TCEP used as an artificial electron donor and this activity requires the Cys motifs binding the Cu atoms and Fe-S clusters.

Discussion

CcoG is the most conserved member of the *ccoGHIS*-encoded cbb_3-Cox assembly proteins and is present in nearly all cbb_3-Cox–containing organisms (Fig. 2). Likewise, relatively few genomes encode a CcoG-like protein without also encoding a cbb_3-Cox (*SI Appendix*, Fig. S8). Earlier on, CcoG was predicted to be a membrane-bound ferredoxin-like protein (31), but its function remained enigmatic for years. Here we show that CcoG is a membrane-integral cupric reductase involved in cbb_3-Cox biogenesis and Cu homeostasis. It is active in anaerobically prepared membranes and can be purified to homogeneity upon detergent solubilization, and the purified protein reduces cupric but not ferric ions in vitro provided that an electron donor is available. Moreover, the Cys motifs of CcoG that bind 2 Cu atoms and 2 [4Fe-4S] clusters are required for its activity, making it a membrane-integral cupric reductase that contains an active site exposed to the cytoplasm.

Cu(II) entering the cytoplasm needs reduction to Cu(I) for efficient delivery to cuproproteins and detoxification via the P_{1B}-type ATPases including CcoI or CopA (27, 38) [or even CopB (39), previously thought to be a Cu(II)-exporting P_{1B}-type ATPase (40)]. Yet, how Cu(II) is reduced in the bacterial cytoplasm was unclear. Its chemical reduction by cytoplasmic glutathione (41), conveying it subsequently to Cu chaperones like Atox1 (a CopZ homolog), has been shown (42). Indeed, glutathione is present in *R. capsulatus* (43) and might contribute to Cu(I) delivery via CopZ to CcoI and CopA (23). However, the Cu(I)–$[GSH]_2$ complex interacts with O_2, forming a Cu(II)–GSSG complex (41), which would render chemical reduction inefficient when the Cu concentrations or cbb_3-Cox demands are high, especially at the onset of respiratory growth. This situation is reminiscent of the enzymatic catalysis of disulfide bonds via the DsbAB system (44). In the oxidizing environment of the periplasm, specific thiol-disulfide oxidoreductases confer rapidity and specificity along or instead of chemical oxidation during protein folding.

Until now, specific cupric reductases have not been described in bacteria. Some enzymes, such as *E. coli* NADH dehydrogenase 2, were shown to reduce Cu(II) in the presence of NADH and either flavin adenine dinucleotide (FAD) or quinol (13). But this activity, like that of *Lactococcus lactis* IL 1403 membranes, was attributed to quinol-mediated chemical Cu(II) reduction (12). Different from bacteria, eukaryotes contain several cupric reductases, often acting primarily as Fe(III) reductases, like the *Saccharomyces*

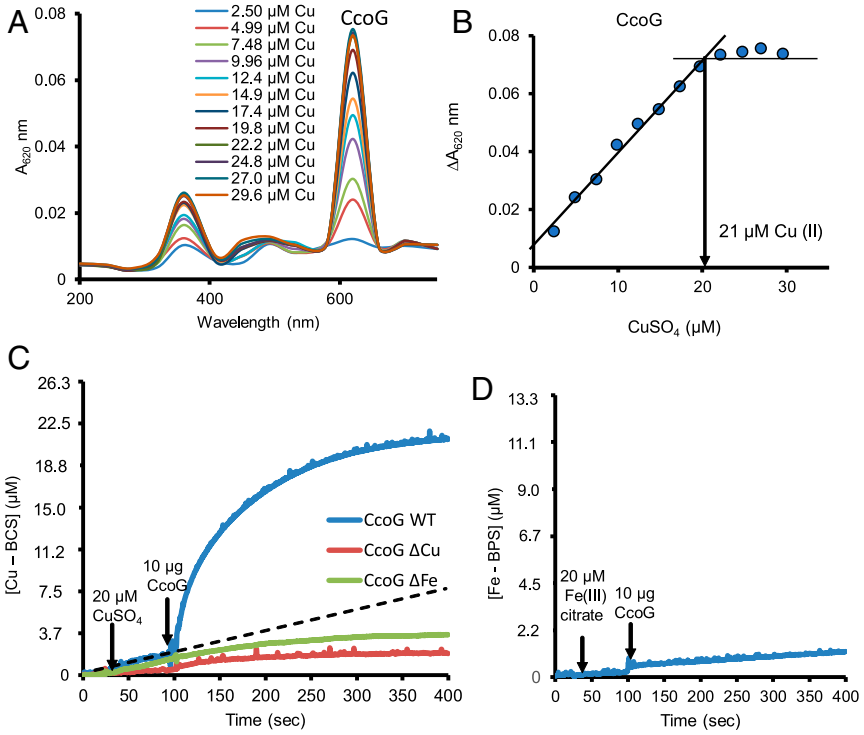

Fig. 6. Purified *R. capsulatus* CcoG binds 2 Cu atoms and has cupric, but not ferric, reductase activity. (*A*) Purified wild-type CcoG protein (12 µM) was incubated with 2.5 to 30 µM $CuSO_4$ and the absorption spectra were recorded between 200 and 800 nm. (*B*) The absorbance values at 620 nm were plotted in function of the $CuSO_4$ concentration used and a stoichiometry of 1:2 for CcoG:Cu(II) was determined. (*C*) Cupric reductase activity of purified CcoG protein was measured anoxically by monitoring the formation of the (Cu–BCS) complex at 482 nm. The Hepes-based assay buffer contained 20 mM Na-citrate, 200 µM BCS, 10 µM TCEP, and 100 µg/mL lecithin. The assay was initiated by adding 20 µM $CuSO_4$, followed by 10 µg of purified CcoG to determine sequentially the rates of CcoG-independent and CcoG-dependent (Cu–BCS) formation (*Materials and Methods*). The dotted line indicates the rate of CcoG-independent Cu(II) reduction (by TCEP) under the conditions used. Unlike the wild-type protein, purified CcoG mutant variants CcoG(ΔCu) and CcoG(ΔFe) lacking the Cu-binding and the [4Fe-4S]–binding Cys motifs, respectively, have no cupric reductase activity. (*D*) Ferric reductase activity of purified wild-type CcoG was assayed by monitoring the formation of the [Fe–BPS] complex at 533 nm (*Materials and Methods*). In all cases, at least 2 independent experiments ($n = 2$) were performed.

cerevisiae Fre1p and Fre2p. These enzymes also reduce Cu(II) and are required for Cu uptake via the high-affinity Cu transporter Ctr1 (45). Unlike CcoG, they are membrane-integral *b*-type cytochromes with axially coordinated hemes, use NADPH as a cofactor, and bind FAD (7, 9, 10, 46). Moreover, they reduce Cu(II) on the extracellular side, unlike CcoG that acts on the intracellular side of the membrane.

Unlike the eukaryotic Fe(III) reductases, bacterial assimilatory Fe(III) reductases are primarily cytoplasmic or periplasmic soluble proteins with narrow substrate specificity, and do not accept Cu(II) as a substrate (47). Membrane-bound proteins that contain an Fe(III) reductase domain (FRD) like the α-proteobacterial YedZ family of proteins were described, but their cupric reductase ability is unknown (48). Clearly, no resemblance between CcoG and the eukaryotic Fe/Cu reductases or the prokaryotic FRD-containing assimilatory Fe(III) reductases is obvious. These features make CcoG the founding member of an entirely novel class of specific Cu reductases that are widely present in bacteria.

To our knowledge, the CcoG family members also appear to be unique as they bind both Cu and Fe-S clusters, with the only other known example being the archaeon *A. fulgidus* cytoplasmic Cu chaperone CopZ (16). Currently, the natural electron donor for neither the Fe-S clusters of *A. fulgidus* CopZ nor for *R. capsulatus* CcoG is known, but potential candidates include the cytoplasmic ferredoxin(s), thioredoxin(s), or glutaredoxin(s). Their redox potentials are close to the redox potential of TCEP (49, 50), which worked efficiently as an artificial electron donor for CcoG. For the membrane-integral CcoG, an enticing other possibility is that electrons are provided by the Q/QH_2 pool, as the membrane fractions containing CcoG seem to provide not only the cupric reductase activity but also the electron donor. Accordingly, CcoG would be part of a putative Cu transport assembly line starting with Cu(II) import via CcoA (21), subsequent reduction to Cu(I) by CcoG, and possible loading onto CopZ (23) before conveyance to CcoI for Cu(I) export back across the membrane. In the periplasm, Cu(I) is then delivered for cbb_3-Cox biogenesis via the periplasmic Cu chaperones PccA and SenC (26). At high Cu concentrations, Cu(I) would also be delivered to CopA to sustain homeostasis and Cu detoxification (28) (Fig. 7). Although some of the components of this assembly line may form stable physical complexes, the interaction between Cu chaperones and their target proteins is generally only very transient and difficult to observe (51).

In conclusion, this study establishes the occurrence of a specific cupric reductase in bacteria. Although in *R. capsulatus* and similar species the prototypical CcoG is specialized for cbb_3-Cox biogenesis, the presence of its paralogs in non–cbb_3-Cox neighborhoods and its homologs in bacteria lacking this terminal oxidase suggests that these family members might have broader cellular functions. Moreover, uncharacterized CcoG-like homologs that lack the Ig-like domain but retain the Cu-binding and [4Fe-4S] motifs (e.g., *E. coli* YccM) are even more widely distributed among the prokaryotes. Similar motifs are also found in NosH and NosR, which are often found encoded in gene neighborhoods of Cu-dependent nitrous oxide reductase and its assembly genes. Clearly, future studies will establish the mechanism of function of this unique class of enzymes, define its natural electron donor, and elucidate why cbb_3-Cox biogenesis requires enzymatic Cu(II) reduction.

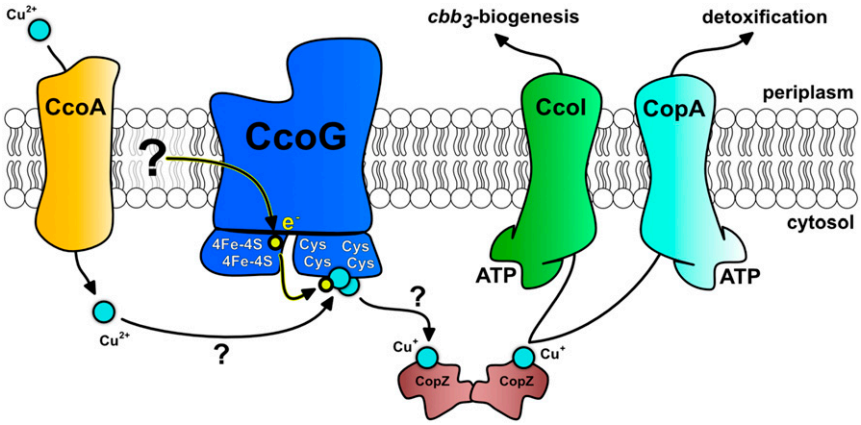

Fig. 7. Working model for the role of CcoG in cbb_3-Cox assembly and Cu homeostasis in *R. capsulatus*. The model depicts the Cu(II) imported by the MFS-type Cu importer CcoA, which is reduced to Cu(I) by CcoG via its [4Fe-4S] clusters and loaded onto CopZ, conveying it to CcoI for cbb_3-Cox biogenesis and to CopA to maintain cellular Cu homeostasis. Cu binding and reduction occur at the 2 Cys motifs via the 2 [4Fe-4S] clusters. The electron donor to CcoG is not known, although the membrane quinone/quinol pool might be a possibility. Arrows with ? indicate the steps that are not yet established experimentally. Accordingly, transient interactions between the components are sufficient for Cu trafficking along the membrane, although some components might form stable complexes.

Materials and Methods

Purification of CcoG from *E. coli* Membranes. For anaerobic purification of CcoG, all buffers were degassed using argon gas and transferred to an anaerobic chamber 1 d prior to usage, and all steps were carried out in sealed vessels or in an anaerobic chamber. An epitope-tagged version of *R. capsulatus* CcoG and its mutated variants was overproduced in the *E. coli* BL21 strain carrying the plasmids pBADccoG$_{Myc\text{-}His}$, pBADccoG$_{Myc\text{-}His}$(ΔCu), and pBADccoG$_{Myc\text{-}His}$(ΔFeS) (*SI Appendix*, Table S2) together with the plasmid pRKISC, kindly provided by Y. Takahashi, Saitama University, Saitama, Japan, harboring the endogenous Fe-S cluster biogenesis (Isc) system, to enhance the Fe-S cluster incorporation (52). Cells were induced with 0.5% L-Ara and 0.1% IPTG at an OD_{600} of 0.5 for 3.5 h and membranes were prepared using a French pressure cell at 16,000 psi in 25 mM Tris·HCl (pH 7.5), 300 mM NaCl, 1 mM Pefabloc, 0.5 mM aminocaproic acid, 30 μg/mL lysozyme, and 30 μg/mL DNase I. After the French press, the cell lysate was centrifuged at 12,500 rpm for 25 min at 4 °C to remove the cell debris and the supernatant was ultracentrifuged for 2 h at 42,000 rpm (118,000 × *g*), 4 °C using a Ti70 rotor. After this step, the membrane pellet was resuspended in precooled ICM buffer (25 mM Tris·HCl, pH 7.5, 150 mM NaCl, 10% glycerol, 1 mM Pefabloc). Membranes were solubilized using the appropriate amounts of a stock solution of 10 mg/mL *n*-dodecyl β-D-maltoside (DDM) at a detergent:protein ratio of 1:1 for 16 h at 4 °C on a rotating wheel. Afterward, the membranes were ultracentrifuged at 42,000 rpm for 1 h at 4 °C using a Ti70 rotor (Beckman Coulter). The supernatant was filtered through a 0.45-μm pore size filter, spiked with 5 mM imidazole and 150 mM NaCl (to reach 300 mM final concentration), and incubated with equilibrated TALON metal affinity resin for 2.5 h at 4 °C according to the manufacturer's recommendations (Clontech Laboratories). The slurry was packed into a 10-mL disposable column and washed 5 times (2.5 mL buffer with 10 mM imidazole each). Proteins were eluted in 6 steps with increasing imidazole concentrations from 20 to 400 mM (1 mL of 20, 40, and 80 mM imidazole followed by 2 × 1 mL of 160, 240, and 400 mM imidazole) using an elution buffer containing 25 mM Tris·HCl (pH 7.5), 300 mM NaCl, 0.05% DDM, 10% glycerol, and 1 mM Pefabloc. The elution buffer was exchanged to the same buffer without imidazole using an Amicon filter Ultra-15 with molecular mass cutoff at 30 kDa and proteins were stored at −80 °C without imidazole.

Binding of Cu to Purified CcoG Protein. Cu binding stoichiometry of CcoG and its variants was determined by visible spectroscopy using the specific metal charge-transfer band observed upon mixing purified CcoG with Cu(II) under aerobic conditions, as described earlier (26). Briefly, the visible spectrum of ∼10 μM purified native or CcoG variants in 25 mM Hepes (pH 7.5) and 150 mM NaCl buffer was recorded between 200 and 750 nm. Using this spectrum as a baseline, spectral changes observed by successive addition of Cu(II) ($CuSO_4$) from 2.5 to 29.6 μM were monitored and the amplitude of A_{620} was normalized to its maximal value, plotted against the Cu(II) concentrations used. The amount of Cu(II) needed to reach binding saturation per amount of protein used yielded the Cu(II):protein binding stoichiometry (26).

Cupric Reductase Assays. The cupric reductase activity was measured spectrophotometrically under anaerobic conditions by monitoring the formation of the Cu(I)–bathocuproine disulfonic acid complex [Cu(I)–BCS2]$^{3-}$ (Cu(I)–BCS) at 482 nm, as adapted from refs. 53 and 54. Anaerobically prepared *R. capsulatus* and *E. coli* membranes from the appropriate strains grown by respiration or purified CcoG proteins (wild-type and variants) were used. Membranes to be assayed were prepared using cell pellets washed with a degassed buffer containing 50 mM Hepes buffer (pH 7.0), 150 mM NaCl, 1 mM dithionite, and 1 mM PMSF. Cells were loaded in an anaerobic chamber into a French pressure cell and, after breakage and centrifugation, all subsequent manipulations were carried out in the anaerobic chamber (Coy). The final washes of membrane pellets used the same buffer without dithionite, and washed membranes were aliquoted and stored frozen at −80 °C. Immediately before use, purified CcoG proteins were exchanged to Hepes buffer (25 mM Hepes, pH 7.0, 300 mM NaCl, 0.05% DDM, 10% glycerol, 1 mM Pefabloc) using a PD MiniTrap G25 column (GE Healthcare). For single-turnover assays, purified CcoG (10 μg per assay) was prereduced by incubation with 4 mM dithionite for 2 h, at 4 °C under anaerobic conditions; dithionite was removed using a PD MiniTrap G25 column (GE Healthcare) with Hepes buffer (25 mM Hepes, pH 7.0, 300 mM NaCl, 10% glycerol, 0.05% DDM, 1 mM Pefabloc). Reduced CcoG was added to a stirring cuvette containing 980 μL of the assay buffer (25 mM Hepes, pH 7.0, 300 mM NaCl, 20 mM Na-citrate, 200 μM BCS). The cuvette was sealed under anaerobic conditions and transferred to the spectrophotometer, the baseline was recorded at 482 nm for 20 to 40 s, 20 μM $CuSO_4$ (20 μL) was injected using an air-tight syringe to start the reaction, and the formation of the Cu(I)–BCS complex was monitored for 3 min with continuous stirring. For the steady-state assays, the same assay buffer was used except that it also contained 10 μM TCEP, 100 μg/mL lecithin, and purified CcoG (10 μg in 25 mM Hepes, pH 7.0, 300 mM NaCl, 10% glycerol, 0.05% DDM, 1 mM Pefabloc), which was not prereduced. The experimental procedure was the same as above when the reaction was started by the addition of $CuSO_4$ (20 μM) and Cu(I)–BCS complex formation was monitored. As needed, in order to determine the chemical rate of Cu(II) reduction by TCEP, first $CuSO_4$ and then CcoG were added and the rates were recorded. For the assays, all manipulations were carried out in the anaerobic chamber, degassed buffers and sealed cuvettes were used, and absorption changes at 482 nm were monitored for Cu(I)–BCS complex formation up to 400 s, or longer as needed. The rate of Cu(II)-to-Cu(I) reduction was determined using the extinction coefficient of 13.300 $M^{-1}\cdot cm^{-1}$ of the Cu(I)–BCS complex (55). The cupric reductase activity associated with CcoG was calculated as nmol of Cu(I) formed per min/μg of membrane proteins or purified CcoG proteins.

Ferric Reductase Assays. Ferric reductase assays were carried out like the cupric reductase assays except that bathophenanthroline disulfonate was used to monitor the formation of the [Fe^{2+}–BPS_3] (Fe–BPS) complex at 533 nm and an extinction coefficient of 22.400 $M^{-1}\cdot cm^{-1}$ was used to determine the ferric reductase activity (56).

Phylogenomic Analysis. The protein similarity network was constructed using the EFI-EST tool (https://efi.igb.illinois.edu/efi-est/) (57, 58) with an alignment score of 100 and nodes were collapsed at a sequence identity of 80%. A full list of identified CcoG-like proteins is available in Dataset S1. The network was visualized with the yFiles organic layout provided with the Cytoscape software (https://www.cytoscape.org) (59). For the phylogenetic analysis, proteins were selected from UniProt (60) reference proteomes based on the presence of the InterPro domain IPR014116 (61). These proteins were then mapped onto UniRef50 clusters and a single representative from each UniRef50 cluster that belonged to a reference proteome was chosen at random for the phylogenetic analysis, which was performed using the CIPRES web portal (62) with MAFFT on XSEDE (v. 7.305) for the sequence alignment (63) and IQ with 1,000 bootstrap replicates (64). Branches with less than 50% bootstrap support were deleted. Gene neighborhoods (a window of 10 genes upstream and downstream of each gene encoding a CcoG-like protein) were retrieved using the EFI-GNT tool (https://efi.igb.illinois.edu/efi-gnt/) (65). A 10-gene window on either side of the *ccoG-like* gene was analyzed for genes encoding a CcoN-like protein (defined as belonging to PF00115), CcoO-like protein (defined as belonging to PF02433), CcoP-like protein (defined as belonging to either PF13442 or PF14715), CcoH-like protein (defined as belonging to PF05751), CcoI-like protein (defined as belonging to PF00122 and either PF00403 or PF12156), CcoQ-like protein (defined as belonging to PF05545), or CcoS-like protein (defined as belonging to PF03597). The presence of a CcoN-like protein in the proteome was defined by detection of InterPro domain IPR004677.

Statistical Analysis. The data are presented as means ± SD in bar charts. The data for enzymatic assays are presented as means, but the SD was omitted for improving visibility. In general, the SD of these assays was below 10%. Statistical analysis was performed using the Student's *t* test and the level of significance is indicated in the figure legends.

ACKNOWLEDGMENTS. We thank Prof. Takahashi, Saitama University for providing the plasmid pRKISC. This work was supported by grants from the Deutsche Forschungsgemeinschaft (DFG GRK2202-235777276/RTG and IRTG1478 to H.-G.K. and T.F.; Project 403222702-SFB 1381 to H.-G.K.); Motivate College of the University Freiburg Medical School and the Erwin Riesch Foundation (D.M.); Deutsche Akademische Austauschdienst (DAAD) (P.-I.T.); partly by the Office of Biological and Environmental Research of the Department of Energy (C.E.B.-H.); partly by the Division of Chemical Sciences, Geosciences and Biosciences, Office of Basic Energy Sciences of the Department of Energy (DOE DE-FG02-91ER20052); and partly by National Institutes of Health (NIH GM 38237) grants (to F.D.). S.S. carried out the ICP-MS analyses that was supported by NIH Grant GM42143 to Sabeeha Merchant, University of California, Berkeley.

1. A. K. Boal, A. C. Rosenzweig, Structural biology of copper trafficking. *Chem. Rev.* **109**, 4760–4779 (2009).
2. L. J. Stewart *et al*., Handling of nutrient copper in the bacterial envelope. *Metallomics* **11**, 50–63 (2019).
3. L. M. Gaetke, C. K. Chow, Copper toxicity, oxidative stress, and antioxidant nutrients. *Toxicology* **189**, 147–163 (2003).
4. K. P. Kepp, A quantitative scale of oxophilicity and thiophilicity. *Inorg. Chem.* **55**, 9461–9470 (2016).
5. L. Macomber, J. A. Imlay, The iron-sulfur clusters of dehydratases are primary intracellular targets of copper toxicity. *Proc. Natl. Acad. Sci. U.S.A.* **106**, 8344–8349 (2009).
6. S. M. Lynch, B. Frei, Mechanisms of copper- and iron-dependent oxidative modification of human low density lipoprotein. *J. Lipid Res.* **34**, 1745–1753 (1993).
7. D. J. Kosman, The teleos of metallo-reduction and metallo-oxidation in eukaryotic iron and copper trafficking. *Metallomics* **10**, 370–377 (2018).
8. E. M. Rees, D. J. Thiele, Identification of a vacuole-associated metalloreductase and its role in Ctr2-mediated intracellular copper mobilization. *J. Biol. Chem.* **282**, 21629–21638 (2007).
9. S. Wyman, R. J. Simpson, A. T. McKie, P. A. Sharp, Dcytb (Cybrd1) functions as both a ferric and a cupric reductase in vitro. *FEBS Lett.* **582**, 1901–1906 (2008).
10. R. S. Ohgami, D. R. Campagna, A. McDonald, M. D. Fleming, The Steap proteins are metalloreductases. *Blood* **108**, 1388–1394 (2006).
11. A. C. Rosenzweig, T. V. O'Halloran, Structure and chemistry of the copper chaperone proteins. *Curr. Opin. Chem. Biol.* **4**, 140–147 (2000).
12. H. K. Abicht, Y. Gonskikh, S. D. Gerber, M. Solioz, Non-enzymic copper reduction by menaquinone enhances copper toxicity in *Lactococcus lactis* IL1403. *Microbiology* **159**, 1190–1197 (2013).
13. V. A. Rapisarda, L. R. Montelongo, R. N. Farías, E. M. Massa, Characterization of an NADH-linked cupric reductase activity from the *Escherichia coli* respiratory chain. *Arch. Biochem. Biophys.* **370**, 143–150 (1999).
14. L. Rodríguez-Montelongo, S. I. Volentini, R. N. Farías, E. M. Massa, V. A. Rapisarda, The Cu(II)-reductase NADH dehydrogenase-2 of *Escherichia coli* improves the bacterial growth in extreme copper concentrations and increases the resistance to the damage caused by copper and hydroperoxide. *Arch. Biochem. Biophys.* **451**, 1–7 (2006).
15. M. Solioz, *Copper and Bacteria: Evolution, Homeostasis and Toxicity* (Springer, 2018).
16. M. H. Sazinsky *et al*., Characterization and structure of a Zn^{2+} and [2Fe-2S]-containing copper chaperone from *Archaeoglobus fulgidus*. *J. Biol. Chem.* **282**, 25950–25959 (2007).
17. A. L. Ducluzeau, S. Ouchane, W. Nitschke, The cbb3 oxidases are an ancient innovation of the domain bacteria. *Mol. Biol. Evol.* **25**, 1158–1166 (2008).
18. B. Khalfaoui-Hassani *et al*., Widespread distribution and functional specificity of the copper importer CcoA: Distinct Cu uptake routes for bacterial cytochrome *c* oxidases. *MBio* **9**, e00065-18 (2018).
19. A. Peters, C. Kulajta, G. Pawlik, F. Daldal, H. G. Koch, Stability of the cbb3-type cytochrome oxidase requires specific CcoQ-CcoP interactions. *J. Bacteriol.* **190**, 5576–5586 (2008).
20. G. Pawlik *et al*., The putative assembly factor CcoH is stably associated with the cbb3-type cytochrome oxidase. *J. Bacteriol.* **192**, 6378–6389 (2010).
21. S. Ekici, H. Yang, H. G. Koch, F. Daldal, Novel transporter required for biogenesis of cbb3-type cytochrome *c* oxidase in *Rhodobacter capsulatus*. *MBio* **3**, e00293-11 (2012).
22. B. Khalfaoui-Hassani, A. F. Verissimo, H. G. Koch, F. Daldal, Uncovering the transmembrane metal binding site of the novel bacterial major facilitator superfamily-type copper importer CcoA. *MBio* **7**, e01981-15 (2016).
23. M. Utz *et al*., The Cu chaperone CopZ is required for Cu homeostasis in *Rhodobacter capsulatus* and influences cytochrome cbb_3 oxidase assembly. *Mol. Microbiol.* **111**, 764–783 (2019).
24. M. González-Guerrero, D. Raimunda, X. Cheng, J. M. Argüello, Distinct functional roles of homologous Cu^+ efflux ATPases in *Pseudomonas aeruginosa*. *Mol. Microbiol.* **78**, 1246–1258 (2010).
25. E. Lohmeyer *et al*., The ScoI homologue SenC is a copper binding protein that interacts directly with the cbb_3-type cytochrome oxidase in *Rhodobacter capsulatus*. *Biochim. Biophys. Acta* **1817**, 2005–2015 (2012).
26. P. I. Trasnea *et al*., A copper relay system involving two periplasmic chaperones drives cbb_3-type cytochrome *c* oxidase biogenesis in *Rhodobacter capsulatus*. *ACS Chem. Biol.* **13**, 1388–1397 (2018).
27. J. M. Argüello, S. J. Patel, J. Quintana, Bacterial Cu(+)-ATPases: Models for molecular structure-function studies. *Metallomics* **8**, 906–914 (2016).
28. S. Ekici *et al*., Intracytoplasmic copper homeostasis controls cytochrome *c* oxidase production. *MBio* **5**, e01055-13 (2014).
29. H. G. Koch, C. Winterstein, A. S. Saribas, J. O. Alben, F. Daldal, Roles of the ccoGHIS gene products in the biogenesis of the cbb_3-type cytochrome *c* oxidase. *J. Mol. Biol.* **297**, 49–65 (2000).
30. C. Kulajta, J. O. Thumfart, S. Haid, F. Daldal, H. G. Koch, Multi-step assembly pathway of the cbb_3-type cytochrome *c* oxidase complex. *J. Mol. Biol.* **355**, 989–1004 (2006).
31. D. Kahn *et al*., *Rhizobium meliloti* fixGHI sequence predicts involvement of a specific cation pump in symbiotic nitrogen fixation. *J. Bacteriol.* **171**, 929–939 (1989).
32. E. L. Neidle, S. Kaplan, *Rhodobacter sphaeroides rdxA*, a homolog of *Rhizobium meliloti* fixG, encodes a membrane protein which may bind cytoplasmic [4Fe-4S] clusters. *J. Bacteriol.* **174**, 6444–6454 (1992).
33. J. H. Roh, S. Kaplan, Genetic and phenotypic analyses of the rdx locus of *Rhodobacter sphaeroides* 2.4.1. *J. Bacteriol.* **182**, 3475–3481 (2000).
34. Y. Zhang *et al*., Cu transport by the extended family of CcoA-like transporters (CalT) in Proteobacteria. *Sci. Rep.* **9**, 1208 (2019).
35. S. Ekici, G. Pawlik, E. Lohmeyer, H. G. Koch, F. Daldal, Biogenesis of cbb_3-type cytochrome *c* oxidase in *Rhodobacter capsulatus*. *Biochim. Biophys. Acta* **1817**, 898–910 (2012).
36. J. Liu *et al*., Metalloproteins containing cytochrome, iron-sulfur, or copper redox centers. *Chem. Rev.* **114**, 4366–4469 (2014).
37. J. A. Imlay, Iron-sulphur clusters and the problem with oxygen. *Mol. Microbiol.* **59**, 1073–1082 (2006).
38. L. Banci *et al*., Affinity gradients drive copper to cellular destinations. *Nature* **465**, 645–648 (2010).
39. R. Purohit *et al*., Cu^+-specific CopB transporter: Revising P_{1B}-type ATPase classification. *Proc. Natl. Acad. Sci. U.S.A.* **115**, 2108–2113 (2018).
40. S. Mana-Capelli, A. K. Mandal, J. M. Argüello, *Archaeoglobus fulgidus* CopB is a thermophilic Cu^{2+}-ATPase: Functional role of its histidine-rich-N-terminal metal binding domain. *J. Biol. Chem.* **278**, 40534–40541 (2003).
41. M. E. Aliaga, C. López-Alarcón, R. Bridi, H. Speisky, Redox-implications associated with the formation of complexes between copper ions and reduced or oxidized glutathione. *J. Inorg. Biochem.* **154**, 78–88 (2016).
42. Y. Hatori, S. Inouye, R. Akagi, Thiol-based copper handling by the copper chaperone Atox1. *IUBMB Life* **69**, 246–254 (2017).
43. K. Li, S. Hein, W. Zou, G. Klug, The glutathione-glutaredoxin system in *Rhodobacter capsulatus*: Part of a complex regulatory network controlling defense against oxidative stress. *J. Bacteriol.* **186**, 6800–6808 (2004).
44. C. Landeta, D. Boyd, J. Beckwith, Disulfide bond formation in prokaryotes. *Nat. Microbiol.* **3**, 270–280 (2018).
45. E. Georgatsou, L. A. Mavrogiannis, G. S. Fragiadakis, D. Alexandraki, The yeast Fre1p/Fre2p cupric reductases facilitate copper uptake and are regulated by the copper-modulated Mac1p activator. *J. Biol. Chem.* **272**, 13786–13792 (1997).
46. A. A. Finegold, K. P. Shatwell, A. W. Segal, R. D. Klausner, A. Dancis, Intramembrane bis-heme motif for transmembrane electron transport conserved in a yeast iron reductase and the human NADPH oxidase. *J. Biol. Chem.* **271**, 31021–31024 (1996).

47. I. Schröder, E. Johnson, S. de Vries, Microbial ferric iron reductases. *FEMS Microbiol. Rev.* **27**, 427–447 (2003).
48. X. Zhang, K. H. Krause, I. Xenarios, T. Soldati, B. Boeckmann, Evolution of the ferric reductase domain (FRD) superfamily: Modularity, functional diversification, and signature motifs. *PLoS One* **8**, e58126 (2013).
49. P. K. Pullela, T. Chiku, M. J. Carvan, III, D. S. Sem, Fluorescence-based detection of thiols in vitro and in vivo using dithiol probes. *Anal. Biochem.* **352**, 265–273 (2006).
50. E. S. Arner, A. Holmgren, Physiological functions of thioredoxin and thioredoxin reductase. *Eur. J. Biochem.* **267**, 6102–6109 (2000).
51. L. Banci *et al*., Copper(I)-mediated protein-protein interactions result from suboptimal interaction surfaces. *Biochem. J.* **422**, 37–42 (2009).
52. H. Huang *et al*., Heterologous overproduction of 2[4Fe4S]- and [2Fe2S]-type clostridial ferredoxins and [2Fe2S]-type agrobacterial ferredoxin. *Protein Expr. Purif.* **121**, 1–8 (2016).
53. R. Hassett, D. J. Kosman, Evidence for Cu(II) reduction as a component of copper uptake by *Saccharomyces cerevisiae*. *J. Biol. Chem.* **270**, 128–134 (1995).
54. K. L. Hill, R. Hassett, D. Kosman, S. Merchant, Regulated copper uptake in *Chlamydomonas reinhardtii* in response to copper availability. *Plant Physiol.* **112**, 697–704 (1996).
55. Z. Xiao, F. Loughlin, G. N. George, G. J. Howlett, A. G. Wedd, C-terminal domain of the membrane copper transporter Ctr1 from *Saccharomyces cerevisiae* binds four Cu(I) ions as a cuprous-thiolate polynuclear cluster: Sub-femtomolar Cu(I) affinity of three proteins involved in copper trafficking. *J. Am. Chem. Soc.* **126**, 3081–3090 (2004).
56. T. Hirayama, H. Nagasawa, Chemical tools for detecting Fe ions. *J. Clin. Biochem. Nutr.* **60**, 39–48 (2017).
57. H. J. Atkinson, J. H. Morris, T. E. Ferrin, P. C. Babbitt, Using sequence similarity networks for visualization of relationships across diverse protein superfamilies. *PLoS One* **4**, e4345 (2009).
58. J. A. Gerlt *et al*., Enzyme Function Initiative-Enzyme Similarity Tool (EFI-EST): A web tool for generating protein sequence similarity networks. *Biochim. Biophys. Acta* **1854**, 1019–1037 (2015).
59. P. Shannon *et al*., Cytoscape: A software environment for integrated models of biomolecular interaction networks. *Genome Res.* **13**, 2498–2504 (2003).
60. UniProt Consortium, UniProt: A worldwide hub of protein knowledge. *Nucleic Acids Res.* **47**, D506–D515 (2019).
61. A. L. Mitchell *et al*., InterPro in 2019: Improving coverage, classification and access to protein sequence annotations. *Nucleic Acids Res.* **47**, D351–D360 (2019).
62. M. A. Miller, W. Pfeiffer, T. Schwartz, "Creating the CIPRES Science Gateway for inference of large phylogenetic trees" in *Proceedings of the Gateway Computing Environments Workshop* (Institute of Electrical and Electronics Engineering (IEEE), New Orleans, 2010), pp 1–8.
63. K. Katoh, D. M. Standley, MAFFT multiple sequence alignment software version 7: Improvements in performance and usability. *Mol. Biol. Evol.* **30**, 772–780 (2013).
64. L. T. Nguyen, H. A. Schmidt, A. von Haeseler, B. Q. Minh, IQ-TREE: A fast and effective stochastic algorithm for estimating maximum-likelihood phylogenies. *Mol. Biol. Evol.* **32**, 268–274 (2015).
65. R. Zallot, N. O. Oberg, J. A. Gerlt, 'Democratized' genomic enzymology web tools for functional assignment. *Curr. Opin. Chem. Biol.* **47**, 77–85 (2018).